RSC Advances

PAPER

View Article Online
View Journal | View Issue

Cite this: *RSC Adv.*, 2017, **7**, 7758

Tungsten doped VO_2/microgels hybrid thermochromic material and its smart window application

Yong-Sheng Yang,†[ab] Yang Zhou,†[b] Freddy Boey Yin Chiang*[b] and Yi Long*[b]

Received 3rd October 2016
Accepted 10th November 2016

DOI: 10.1039/c6ra24686a

www.rsc.org/advances

Thermal sensitive microgels were synthesized directly from hydroxypropyl cellulose (HPC) and acrylic acid (AA) in pure water. The first cloud point temperature, near 45 °C, of the inorganic/organic hybrid thermochromic material was obtained by dispersing W doped VO_2 in HPCA microgels and the composite microgel is highly transparent at room temperature with T_{lum} = 80% when the thickness is 25 μm. The excellent solar modulating ability (ΔT_{sol}) of 36%, high averaged T_{lum} of 56% and relatively high cloud point temperature of 50 °C make it suitable for smart windows applications compared with pure VO_2 based materials and previously reported thermochromic hybrids.

Introduction

Due to the zero extra energy requirement and large solar spectrum wavelength blocking effect, thermochromic materials have become the cost effective smart window material. For an ideal thermochromic smart-window, a large solar modulation, ΔT_{sol}, a suitable critical temperature (τ_c) and a relatively high luminous transmission (T_{lum}) are required.[1] Vanadium dioxide (VO_2) is the most studied thermochromic material in the energy-saving smart window applications. The phase transition critical temperature is around 68 °C and the VO_2 can block infrared (IR) transmission (T_{IR}) at a temperature above τ_c and allow IR transmission below τ_c.[2,3] To attain good thermochromic properties, much effort, such as doping (such as Mg^{2+}/W, and rare earth doping, such as Tb, La and Eu^{3+}),[3–7] nanoporous reconstruction,[8] antireflective coating multilayers,[9,10] nanoparticle-based composites,[11–15] and gridded[16] and biomimetic nanostructuring[17,18] have been investigated. However, the intrinsic physical properties of VO_2 of a high τ_c of 68 °C restricted it to be applied directly to smart windows applications. Doping by tungsten can significantly reduce τ_c of VO_2 nanoparticles.[3]

Hydroxypropylcellulose (HPC) is a water-soluble cellulose derivative,[19] which has being developed into materials such as for environmental friendly and biocompatible requirements,[20] and biodegradable, non-toxic and solid polymers.[21] As a renewable resource, HPC also has a number of traditional applications including in the biological, medical and pharmaceutical fields.[22–28]

In previous work, a thermochromic material based on HPC has been reported.[29] In this paper, a facile way of preparing a HPC derivative (HPCA microgel) based thermochromic material is reported. By hybridizing with W doped-VO_2 nanoparticles, HPC offers both a large visible and IR modulating ability together with a relative high T_{lum}. This is the first near room temperature hybrid thermochromic material.

Experimental

Materials

The chemicals used in this study were HPC (MW 100 000, 99% purification, Sigma-Aldrich), W-VO_2 (Jing Cheng PTE LTD), acrylic acid (AA) (Sigma-Aldrich), Disperbyk 180 (Sigma-Aldrich) and a multipurpose sealant (Selleys All Clear). AA was dried by $MgSO_4$ and then vacuum distilled before use. *N*,*N*′-Methylene bisacrylamide (MBA) (Fluka) was recrystallized from methanol. Cerium(IV) ammonium nitrate (CAN) (Sigma-Aldrich) was recrystallized from dilute nitric acid containing an appropriate amount of ammonium nitrate. Deionized water (18.2 MΩ) was used throughout the experiments. All chemicals were used as received, without any further purification.

Synthesis of HPCA microgel

An aqueous solution of 50 mg CAN in 2.5 mL of 0.1 mol L^{-1} nitric acid and 0.7 mL of AA were successively added to 100 mL of 2% aqueous solution of HPC under gentle stirring and nitrogen bubbling. The reaction proceeded at 25 °C for 1 h, then 15 mL AA and 5 g MBA were added, stirred for a further 4 h with pH kept at 1–2, followed by adjusting the pH to 7.0 with 3 mol L^{-1} NaOH. Excess precursors and side-products were removed

[a]School of Chemistry and Engineering, Wuhan Textile University, 1 Textile Road, Wuhan, 430073, China

[b]School of Materials Science and Engineering, Nanyang Technological University, 50 Nanyang Avenue, Singapore 639798. E-mail: mycboey@ntu.edu.sg; longyi@ntu.edu.sg

† The authors equally contributed to this paper.

over 7 days of dialysis using a membrane bag with a molecular weight cutoff of 14 000. The resultant microgels were obtained by freeze-drying the remaining solvent in the membrane bag. The synthesis procedure is illustrated in Scheme 1.

Preparation of HPCA microgel films

A 0.03 g HPCA sample was mixed in 2 mL deionized water to form the HPCA microgel by ultrasonics for one hour to ensure it thoroughly dissolved and was left to stand for one day to form the microgel.

Preparation of W-doped VO_2 film

The W-doped VO_2/DPM solution was prepared by dilution with a DPM solution with a volume ratio of 1 : 10. Samples with a 25 μm thickness film were made, the same as W-doped VO_2/HPCA microgel films.

Preparation of W-doped VO_2/HPCA microgel composite films

The dispersion of W-doped VO_2 (Jing Cheng PTE LTD) into hydrogel has been previously reported.[30,31] 0.05 g W-doped VO_2 nanoparticles was added into the 0.5 mL DPM solution; after 30 minutes of ultrasonic dispersion, 5 μL BYK 180 was added into the solution, then dispersed in ultrasonics for 30 minutes more. The W-VO_2 solution was mixed with the HPCA solution with a volume ratio of 1 : 10. Samples with 12.5 μm, 25 μm and 50 μm films were made and the sealant was applied at the edges to prevent mass exchange with the outside environment.

Characterization

SEM. The inner structures of the HPCA were determined by a field emission scanning electron microscope (FESEM, SUPRA 55, ZEISS) with an operating voltage of 5.00 kV. 2 mL HPCA solution was injected into 2 plastic vials separately and equally, one vial was heated to 80 °C for 5 minutes and the two vials were immersed into nitrogen liquid immediately. The 2 samples were then freeze-dried and examined by SEM.

UV-VIS-NIR. Optical properties were examined by UV-VIS-NIR (Cary 5000, Agilent, USA) spectra, with a working wavelength range of 250–2500 nm at 10 nm s^{-1} incidence. All the tests were run at 20 °C and 60 °C, respectively, while the temperature was controlled by a heating stage (PE120, Linkam, UK). The calculation of the integral luminous transmittance, T_{lum} (380–780 nm), infrared transmittance, T_{IR} (780–2500 nm) and solar transmittance, T_{sol} (250–2500 nm) and $\Delta T_{lum/IR/sol}$ can be found elsewhere.[32]

The integral luminous transmittance T_{lum} (380–780 nm), IR transmittance T_{IR} (780–2500 nm), and solar transmittance T_{sol} (250–2500 nm) were calculated with eqn (1):

$$T_{lum}/IR/sol = \frac{\int \varphi_{lum}/IR/sol(\lambda)T(\lambda)d\lambda}{\int \varphi_{lum}/IR/sol(\lambda)T(\lambda)d\lambda} \quad (1)$$

where $T(\lambda)$ denotes spectral transmittance, $\varphi_{lum}(\lambda)$ is the standard luminous efficiency function of photopic vision[33] in the wavelength range of 380–780 nm, and $\varphi_{IR}(\lambda)$ and $\varphi_{sol}(\lambda)$ are the IR/solar irradiance spectrum distribution for air mass 1.5 (corresponding to the sun standing 37° above the horizon with 1.5 atmosphere thickness and the presence of a solar zenith angle of 48.2).[34] $\Delta T_{lum/IR/sol}$ is obtained by $\Delta T_{lum/IR/sol} = T_{lum/IR/sol,20\ °C} - T_{lum/IR/sol,60\ °C}$.

Results and discussion

As shown in Fig. 1a, the transmission in the visible range of pure HPCA microgel dramatically decreases when the temperature changes from 20 °C to 65 °C with a negligible IR change. The T_{lum} of the sample reduced from almost 85% to less than 40%, which reflected that the solution changes from transparent at 20 °C to translucent at 50 °C (see the glass film in Fig. 1b). It can be recovered to transparency within 1 min after removing the heater. The reduction in transmittance at around 1430 and 1930 nm for both high and low temperatures is due to the absorption of water at these two wavelengths.

The HPC hydrogels at both 20 and 80 °C were freeze-dried and the remaining solid was examined by SEM. Fig. 2 shows the difference in the structure of HPCA at 20 and 80 °C; the polymer fibers at room temperature are more elongated and uniform (Fig. 2a); however, at 80 °C, the length of the polymer fibers is reduced dramatically to around 4–5 μm, accompanied by a largely contracted pore size of less than 8 μm (Fig. 2b). The water driven out from the HPCA microgel fiber above the cloud point temperature causes the shrinkage; the much more complicated polymeric web structure acts as a scattering center to block the visible light and results in an opaque status above the cloud point temperature.

The transmittance at a fixed wavelength of 580 nm in the temperature range 20 to 65 °C was recorded in a heating and cooling cycle and plotted as %*T versus T*/°C hysteresis loops for

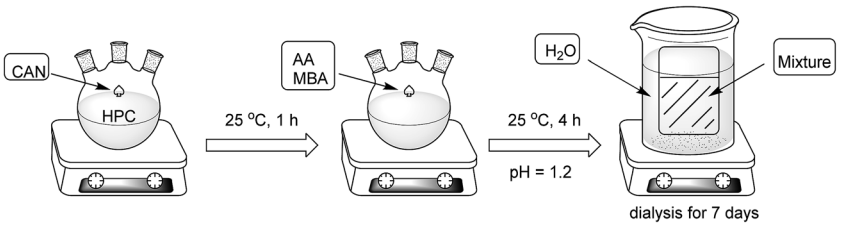

Scheme 1 Scheme of synthesizing HPCA microgel.

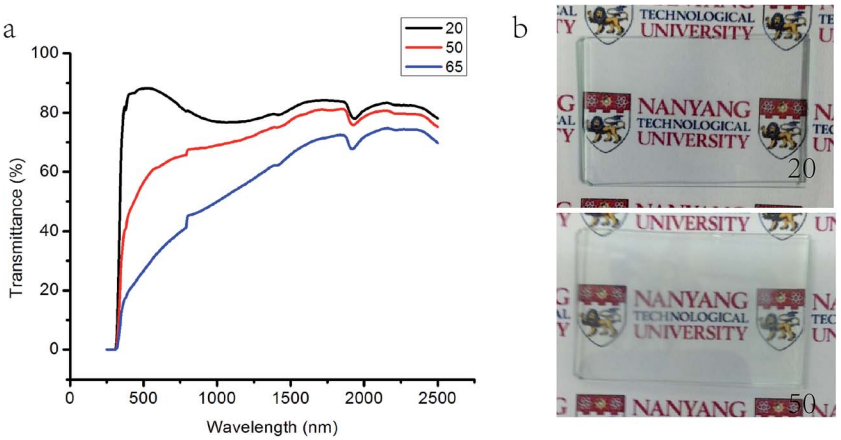

Fig. 1 (a) Optical transmittance spectra of the 25 μm HPCA microgel sample with temperatures from 20 °C to 65 °C. (b) Pictures of 20 °C and 50 °C HPCA microgels.

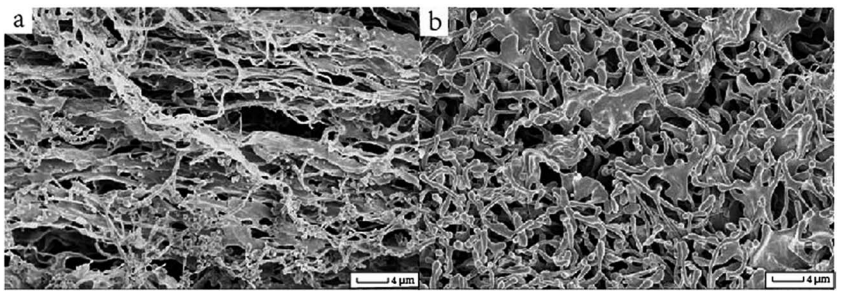

Fig. 2 SEM image of the freeze-dried HPCA microgel at (a) 20 °C and (b) 80 °C.

pure HPCA and W-VO_2 HPCA composite microgels, with a fixed wavelength for W-VO_2 of 2500 nm (Fig. 3). The transmission electron microscope (TEM) image of the particles is shown in the inset, indicating that the particle size is in the order of 50 nm. The cloud point temperature of pure HPCA is about 52.5 °C and τ_c for the W-VO_2 is 40 °C on average for the cooling and heating cycle with a T_{lum} decrease from 70% to 45% when the temperature rose from 25 °C to 65 °C. It is of great interest that W-VO_2 can reduce the cloud point temperature of HPCA to 50 °C, which indicates that W doped VO_2 could influence the phase change of the HPCA microgel.

The thickness influence on ΔT_{sol}, ΔT_{lum}, and ΔT_{IR} was investigated in this work. The optical transmittance spectra of 12.5, 25 and 50 μm thickness of the HPCA microgel samples are shown in Fig. 4a; and the $T_{lum(20,60\ °C)}$, ΔT_{sol}, ΔT_{lum}, and ΔT_{IR} are shown in Fig. 4b. The T_{lum} of 20 °C of the HPCA film slightly decreases from 87.5% to 85.1%; however, the T_{lum} of 60 °C of HPCA film dramatically drops from 49.2% to 22.9%. The ΔT_{sol}, ΔT_{lum}, and ΔT_{IR} increase slightly from 12.5 μm to 25 μm and increase dramatically from 25 μm to 50 μm. Although the 50 μm thick HPCA microgel exhibits a much higher ΔT_{sol} value of 44%, its low $T_{lum(60\ °C)}$ of less than 25% is not favored for an ideal smart window.

According to the above discussion, the pure HPCA microgel of 25 μm thickness was the most suitable for smart windows application compared with 12.5 and 50 μm. The optical transmittance spectra of 25 μm thickness samples of HPCA, W-VO_2, and W-VO_2 HPCA composite microgel (250–2500 nm) profiles at 20 °C and 60 °C are shown in Fig. 4c. The pure HPCA film has the highest solar transmittance for a temperature of 20 °C with a T_{lum} of 87%. The ΔT_{lum} of the pure HPCA microgel is 43%, which indicates that when the temperature rises up to 60 °C, the transmittance of the sample turns opaque. For pure W-VO_2, the large transmission contrast remains in the IR region, the ΔT_{IR} is up to 15% compared to a ΔT_{sol} of 5%, so it serves as a good smart IR blocking additive in the HPCA microgel. Although adding W-VO_2 lowers the transmittance at both 20 °C and 60 °C, as adding W-VO_2 into HPCA thin film forms a hybrid, the ΔT_{IR} of the hybrid increased 2 times from 12 to 24% compared with that of the pure HPCA film (Fig. 4d), while ΔT_{lum} also increased from 42.6 to 47.5%, which led to a 25.5% increase of ΔT_{sol}. Thus, the new hybrid has a larger modulating ability in both the visible and IR ranges compared with pure HPCA and W-VO_2 film; at the same time, a dramatically high $\Delta T_{sol} \sim 36.4\%$ was achieved with just 7.2% of visible transmittance sacrificed at room temperature. This is the first device which can effectively block both visible and IR light with a suitable phase change temperature.

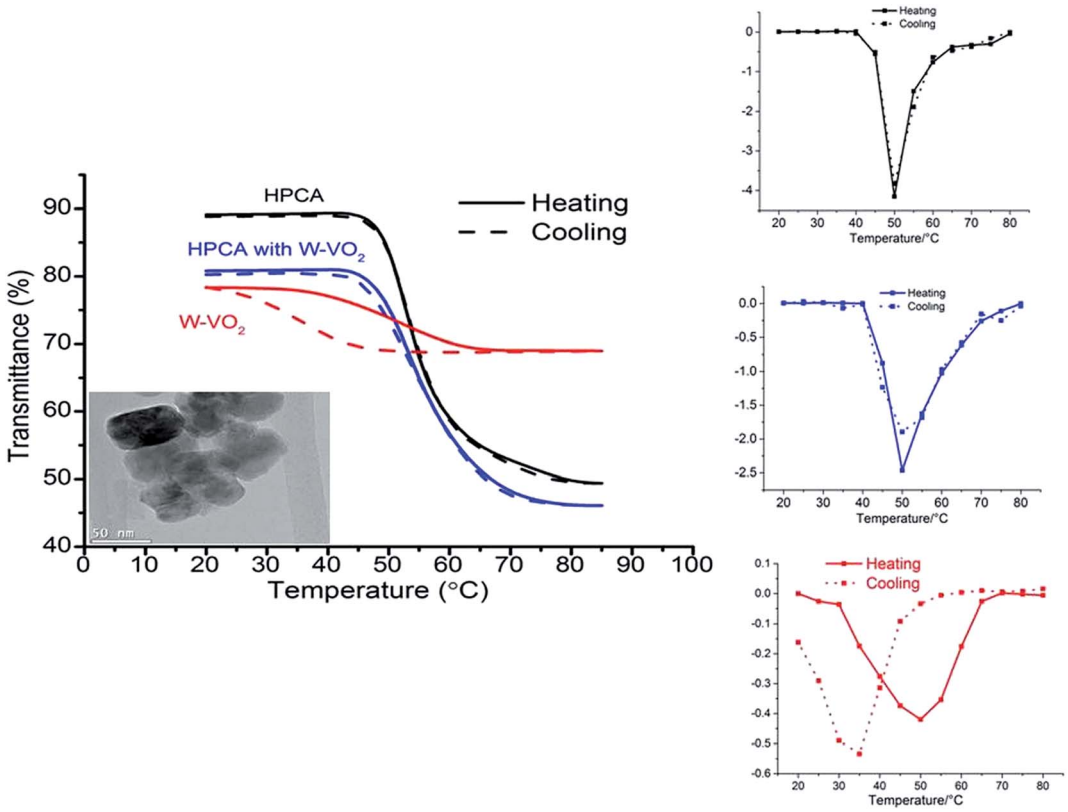

Fig. 3 Hysteresis loops for the temperature-dependent transmittance of the HPCA and W-VO_2 HPCA composite microgels of 12.5 μm thickness at a wavelength of 580 nm and W-VO_2 nanoparticles of 12.5 μm thickness at a wavelength of 2500 nm with the corresponding derivative on the right. Inset: TEM picture of W-VO_2 nanoparticles.

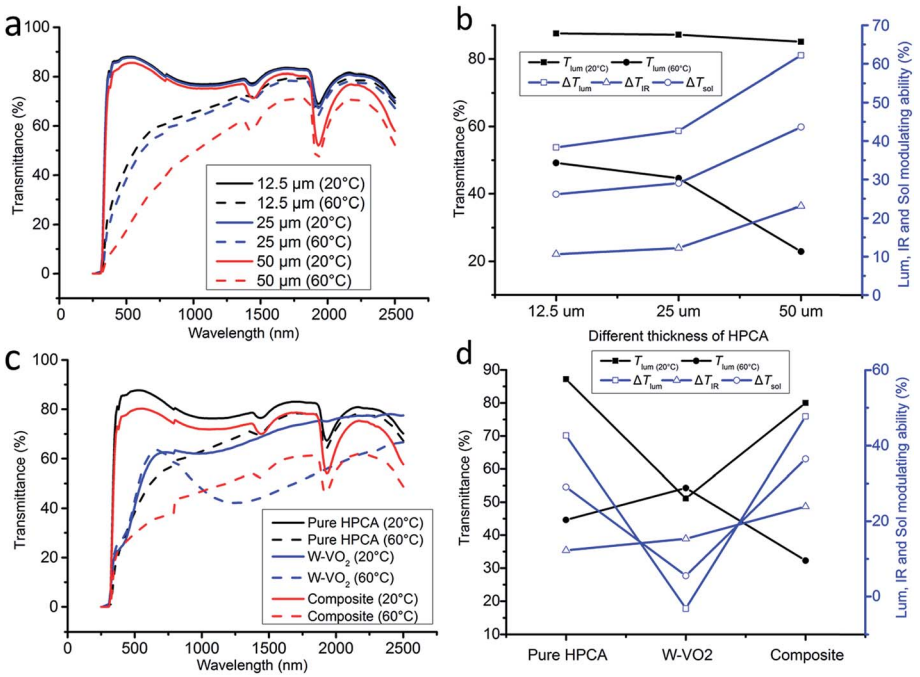

Fig. 4 (a) Optical transmittance spectra of 12.5, 25 and 50 μm thick HPCA microgel samples; (b) thickness influence on ΔT_{sol}, ΔT_{lum}, ΔT_{IR} and T_{lum} (20 and 60 °C) of HPCA samples; (c) optical transmittance spectra of 25 μm HPCA, W-VO_2, and W-VO_2 with HPCA microgel samples. (d) ΔT_{sol}, ΔT_{lum}, ΔT_{IR} and T_{lum} (20 and 60 °C) of 25 μm HPCA, W-VO_2, and W-VO_2 with HPCA microgel samples.

Conclusion

A temperature-responsive HPCA microgel has been synthesized and W-VO_2 nanoparticles were hybridized to this microgel. The 25 μm thickness composite microgel could be totally transparent at room temperature, with a high T_{lum} of 80%, and turned translucent at 60 °C, with an acceptable T_{lum} of 33%. The luminous contrast contributed from HPCA combined with the IR transmission contrast due to the W-VO_2 give a high ΔT_{sol} of 36%. The SEM of the room temperature and high temperature samples indicated that the polymer fiber became more diminished and the pores became smaller, and this polymeric web structure acts as a scattering center to block the visible light and result in an opaque status at high temperature.

Acknowledgements

This research is supported by the Singapore Minster of Education (MOE) Academic Research Fund Tier 1 RG101/13 and NRF2015NRF-POC002-019 and the fund of Wuhan Textile University (017/165006).

References

1 S.-Y. Li, G. A. Niklasson and C. G. Granqvist, *J. Appl. Phys.*, 2010, **108**, 063525.
2 Z. Zhang, Y. Gao, Z. Chen, J. Du, C. Cao, L. Kang and H. Luo, *Langmuir*, 2010, **26**, 10738–10744.
3 N. Wang, M. Duchamp, R. E. Dunin-Borkowski, S. Liu, X. Zeng, X. Cao and Y. Long, *Langmuir*, 2016, **32**, 759–764.
4 N. Wang, S. Y. Liu, X. T. Zeng, S. Magdassi and Y. Long, *J. Mater. Chem. C*, 2015, **3**, 6771–6777.
5 X. Cao, N. Wang, S. Magdassi, D. Mandler and Y. Long, *Sci. Adv. Mater.*, 2014, **6**, 558–561.
6 N. Mlyuka, G. Niklasson and C.-G. Granqvist, *Appl. Phys. Lett.*, 2009, **95**, 171909.
7 N. Wang, M. Duchamp, C. Xue, R. E. Dunin-Borkowski, G. Liu and Y. Long, *Adv. Mater. Interfaces*, 2016, **3**, 1600164.
8 L. Kang, Y. Gao, H. Luo, Z. Chen, J. Du and Z. Zhang, *ACS Appl. Mater. Interfaces*, 2011, **3**, 135–138.
9 C. Liu, N. Wang and Y. Long, *Appl. Surf. Sci.*, 2013, **283**, 222–226.
10 Z. Chen, Y. Gao, L. Kang, J. Du, Z. Zhang, H. Luo, H. Miao and G. Tan, *Sol. Energy Mater. Sol. Cells*, 2011, **95**, 2677–2684.
11 P. Liu, L. A. Liu, K. L. Jiang and S. S. Fan, *Small*, 2011, **7**, 732–736.
12 Z. Chen, C. Cao, S. Chen, H. Luo and Y. Gao, *J. Mater. Chem. A*, 2014, **2**, 11874–11884.
13 Z. Chen, Y. Gao, L. Kang, C. Cao, S. Chen and H. Luo, *J. Mater. Chem. A*, 2014, **2**, 2718–2727.
14 Y. F. Gao, S. B. Wang, L. T. Kang, Z. Chen, J. Du, X. L. Liu, H. J. Luo and M. Kanehira, *Energy Environ. Sci.*, 2012, **5**, 8234–8237.
15 C. Liu, X. Cao, A. Kamyshny, J. Y. Law, S. Magdassi and Y. Long, *J. Colloid Interface Sci.*, 2014, **427**, 49–53.
16 C. Liu, I. Balin, S. Magdassi, I. Abdulhalim and Y. Long, *Opt. Express*, 2015, **23**, A124–A132.
17 X. Qian, N. Wang, Y. Li, J. Zhang, Z. Xu and Y. Long, *Langmuir*, 2014, **30**, 10766–10771.
18 A. Taylor, I. Parkin, N. Noor, C. Tummeltshammer, M. S. Brown and I. Papakonstantinou, *Opt. Express*, 2013, **21**, A750–A764.
19 S. Fortin and G. Charlet, *Macromolecules*, 1989, **22**, 2286–2292.
20 D. Klemm, B. Heublein, H.-P. Fink and A. Bohn, *Angew. Chem., Int. Ed.*, 2005, **44**, 3358–3393.
21 Y. Nishio, *Cellul. Polym., Blends Compos.*, 1994, 5.
22 D. Richardson, E. J. Lindley, C. Bartlett and E. J. Will, *Am. J. Kidney Dis.*, 2003, **42**, 551–560.
23 R. a. Rodríguez, C. Alvarez-Lorenzo and A. Concheiro, *J. Controlled Release*, 2003, **86**, 253–265.
24 J. Siepmann, K. Podual, M. Sriwongjanya, N. Peppas and R. Bodmeier, *J. Pharm. Sci.*, 1999, **88**, 65–72.
25 Y. Suzuki and Y. Makino, *J. Controlled Release*, 1999, **62**, 101–107.
26 M. F. Francis, M. Piredda and F. M. Winnik, *J. Controlled Release*, 2003, **93**, 59–68.
27 C. R. Park and D. L. Munday, *Int. J. Pharm.*, 2002, **237**, 215–226.
28 J. Siepmann and N. Peppas, *Adv. Drug Delivery Rev.*, 2012, **64**, 163–174.
29 Y.-S. Yang, Y. Zhou, F. B. Y. Chiang and Y. Long, *RSC Adv.*, 2016, **6**, 61449–61453.
30 C. Liu, X. Cao, A. Kamyshny, J. Law, S. Magdassi and Y. Long, *J. Colloid Interface Sci.*, 2014, **427**, 49–53.
31 Y. Zhou, Y. Cai, X. Hu and Y. Long, *J. Mater. Chem. A*, 2015, **3**, 1121–1126.
32 Y. Zhou, Y. Cai, X. Hu and Y. Long, *J. Mater. Chem. A*, 2014, **2**, 13550–13555.
33 G. Wyszecki and W. S. Stiles, *Color Science: Concepts and Methods, Quantitative Data and Formulae*, Wiley, New York, 2000.
34 ASTM G173 Standard Tables of Reference, *Solar Spectral Irradiances: Direct Normal and Hemispherical a 37° Tilted Surface, Annual Book of ASTM Standards*, American Society for Testing and Materials, Philadelphia, PA, USA, 2012, vol. 14.04, http://rredc.nrel.gov/solar/spectra.am1.5.

